Origin of the exclusive ternary electroluminescent behavior of BN-doped nanographenes in efficient single-component white light-emitting electrochemical cells

By Elisa Fresta, Jacopo Dosso, Juan Cabanillas-González, Julio Fernandez-Cestau, Davide Bonifazi, and Rubén D. Costa*

Elisa Fresta, Julio Fernandez-Cestau and Dr. Rubén D. Costa*
IMDEA Materials Institute, Calle Eric Kandel 2, E-28906 Getafe, Madrid, Spain.
ruben.costa@imdea.org

Elisa Fresta
Universidad Autónoma de Madrid, Departamento de Física Aplicada, Calle Francisco Tomás y Valiente, 7, 28049 Madrid, Spain.

Jacopo Dosso and Prof. Davide Bonifazi
School of Chemistry, Cardiff University, CF10 3AT Cardiff, Great Britain.

Dr. Juan Cabanillas
IMDEA Nanoscience, Calle Faraday 9, 28049 Madrid, Spain.

Keywords

Small molecules, BN-doped nanographene, ternary electroluminescent mechanism, single-component white lighting, white light-emitting electrochemical cells

Abstract

White light-emitting electrochemical cells (WLECs) still represent a significant milestone, since only a few examples with moderate performances have been reported. Particularly, multi-emissive white emitters are highly desired, as a paradigm to circumvent phase separation and voltage-dependent emission color issues that are encountered following host:guest and multi-layered approaches. Herein, we rationalized the origin of the exclusive white ternary electroluminescent behavior of BN-doped nanographenes with a B_3N_3 doping pattern (hexa-perihexabenzoborazinocoronene), leading to one of the most efficient (~3 cd/A) and stable over days single-component and single-layered WLECs. Up to date, BN-doped nanographenes have featured blue thermally activated delayed fluorescence (TADF). This doping pattern provides, however, white electroluminescence spanning the whole visible range (x/y CIE coordinates of 0.29-31/0.31-38 and average color rendering index (CRI) of 87) through a ternary emission involving fluorescence and thermally activated dual phosphorescence. This temperature dependent multi-emissive mechanism is operative for both photo- and electro-luminescence processes and holds over the device lifespan, regardless of the device architecture, active layer composition, and operating conditions. As such, this work represents a new stepping-stone

towards designing a new family of multi-emissive white emitters based on BN-doped nanographenes that realizes one of the best performing single-component white-emitting devices compared to the prior-art.

1. Introduction

White light-emitting electrochemical cells (WLECs) have recently been attracting much interest as they offer low-cost, single-layer, and air-stable alternatives for lighting applications, such as signaling, panels, and labelling.[1–5] However, efficient and stable single-component and single-layered WLECs still represent a significant milestone.[6–8] Up to date, there are four approaches to fabricate WLECs. First, host:guest active layers mixing a high-energy emitting host with a low-energy emitting guest are subjected to several drawbacks, such as phase separation, poor color stability over time, extreme sensitivity to the layer thickness and the ratio between emitters, as well as voltage-dependent color emission.[9–11] Second, multi-layered architectures based on either tandem or color down-converting schemes suffer from the high production costs due to complicate architectures and the low feasibility to customize tailored emitters.[12,13] A third strategy is to exploit white-emitting excimers or exciplex species.[14,15] This has, however, given poorly efficient devices due to the intrinsic low photoluminescence quantum yields (ϕ) of these emitting species. Finally, the most desired approach is the use of intrinsically white-emitting molecules for single-component WLECs. Up to date, there are a handful number of contributions involving conjugated polymers (CPs)[16,17] and small molecules (SMs).[18,19] Edman and Pei groups have reported excellent examples in CP-WLECs designing emitters with different multifluorophoric units.[16,17] They achieved encouraging LEC performances with efficiencies of *ca*. 3 cd/A, color rendering index (CRI) of *ca*. 80, and stabilities of few hours. Recently, devices with low efficiencies (<0.5 cd/A), CRI of around 90, and stabilities of <1 day have been realized with TIPs-functionalized pentacenes[18] and free-base porphyrins[19] controlling the photo-induced degradation upon film forming and the strength of local electric-fields under operation, respectively.

In parallel, a few groups working in single-component white organic light-emitting diodes (WOLEDs) have unraveled new white emission mechanisms using SMs.[20–22] For instance, Li's group and others have reported on a low-energy electromeric emission that was highly favored upon the influence of the electric field,[20] while Mazzeo *et al.* have reported on the formation of low-energy emitting cross-like dimers upon film forming.[21] Finally, Park and collaborators prepared a white-emitting SM with two fluorophores, in which the energy transfer between them was blocked allowing electroluminescence from both moieties.[22] All-in-all, these examples show similar performances to those of WLECs, achieving high CRI values (70-

85) and efficiencies of *ca.* 1 cd/A. Despite the excellent color features of SM-based lighting devices, the efficiency is highly limited by the low ϕ value in thin-films and the 25% electron-hole recombination yield.

In light of the above mentioned, single-component white-emitting devices based on a multi-emissive electroluminescent response – *i.e.*, equally efficient dual or ternary emission – has not been accomplished yet. Indeed, the molecular design of emitters featuring ternary photoluminescence mechanisms is still in its infancy with one of the very first examples recently reported by Yang and co-workers;[23] though it has not been proven in lighting devices so far. Hence, both the molecular design of multi-emissive compounds and its effective use towards white devices represent one of the most significant milestones in the thin-film lighting field.

In this context, this work provides the first example that fully meets the requirements to open a new approach towards single-component and single-layered white-emitting devices. In short, we deciphered the electroluminescent features of a BN-doped nanographene with the B_3N_3 doping pattern – *i.e.*, hexa-peri-hexabenzoborazinocoronene or **1** as shown in Figure 1 – in thin-films using the LEC concept. Despite its blue fluorescence in both solution and thin-films at room temperature,[24] efficient (*ca.* 3 cd/A) and stable over days WLECs with a broad white spectrum peaking at 435, 505, 550, 695, and 750 nm – *i.e.*, x/y CIE color coordinates of 0.28-0.31/0.31-0.38 and average CRI = 87 – were easily achieved regardless of active layer composition – *i.e.*, type of ion-doped matrix and its interaction with **1** –, device architecture and operation – *i.e.*, thickness, electrodes, and driving conditions. The origin of this exclusive white electroluminescent response is a highly desired multi-emissive mechanism involving a ternary emission that includes fluorescence and a thermally activated dual phosphorescence. This temperature dependent multi-emissive mechanism is an intrinsic feature of **1** as it is operative for both photo- and electro-luminescence processes, holding for the whole device lifespan.

Hence, this work shows an exclusive emission behavior of BN-doped nanographenes with the B_3N_3 doping pattern, leading to one of the most efficient and stable WLECs compared to the prior-art. This will represent a landmark towards the designing a new family of white emitters based on BN-doped nanographenes for highly efficient single-component and single-layered white-emitting devices.

2. Results and Discussion

Capitalizing on the BN-doping approach[24–40] to tailor the physical[24,41–44] and chemical[40,45,46] properties of polycyclic aromatic hydrocarbons (PAHs) and nanographenes, we have recently developed the first rationale synthesis of a B_3N_3-doped nanographene, hexa-peri-hexabenzoborazinocoronene or **1**.[24] The characterization of **1** is provided in a previous contribution[24] and in the Supporting Information. Its purity is confirmed by both ^{1}H-NMR, HPLC (high-performance liquid chromatography) and excitation spectra (Figure S1-3). Please notice that below results were obtained from three batches, confirming the lack of artifacts related to impurities. The photophysical characterization of **1** in solution showed blue fluorescence (wavelength maxima or λ_{max} = 415 nm) and green phosphorescence (λ_{max} = 525 nm) at room temperature and 77 K (Figure S4), respectively. Inspired by recent developments describing the first use of BN-doped molecular materials in electroluminescent devices,[47–50] and the exploitation of thermally activated delayed fluorescence (TADF)[31] in BN-doped nanographene, we engineered LECs containing **1** as the active emitter to elucidate its electroluminescence behavior.

As a first step, we prepared thin-films containing only **1** and mixed with the ionic matrix as those used in devices – *i.e.*, **1**:PS:PEO:LiOTf in a mass ratio 10:0.9:2.6:0.78 being PS (polystyrene), PEO (polyethylene oxide) and LiOTf (Lithium Triflate); see Supporting Information for more details. Atomic Force Microscopy (AFM) assay confirm that both films show a similar homogenous morphology with root-mean-square roughness of 2 nm (Figure 1). Likewise, the photoluminescence features are similar at room temperature and in air, involving a well-structured blue emission band centered at 415 nm (Figure 1), ϕ = 22.1%, and excited state lifetimes (τ) of *ca.* 3 ns (Figure 1).

Next, the electroluminescent behavior **1** was studied in devices built as ITO/PEDOT:PSS(70 nm)/**1**:PS:PEO:LiOTf 10:0.9:2.6:0.78 (100 nm)/Al(90 nm) – see SI for more details on the device preparation. The devices were driven at pulsed current of 5 mA monitoring the luminance, color, and electrical behavior over time. In stark contrast with the blue photoluminescence features of the thin films, these devices exhibit a white electroluminescence response covering the whole visible range (Figure 2). Specifically, the electroluminescence spectral envelop consists of three well-defined peaks located at 435, 505, and 695 nm along with shoulders at 550 and 750 nm that are associated to x/y CIE coordinates of 0.28/0.31 and CRI value of 89. Notably, the shape of the electroluminescence emission changes until the maximum luminance is reached (Figure 2), showing *i*) an intensity decrease

of the high-energy peak (λ_{max} = 435 nm), *ii*) an intensity increase and broadening of the mid-energy peak leading to a red-shifted λ_{max} (530 nm), and *iii*) an intensity increase of the low-energy peak (λ_{max} = 695 nm). This results in a peak intensity pattern that corresponds to final x/y CIE coordinates of 0.31/0.38 and CRI of 85 holding until the devices is dead (Figure 2). Despite of the changes of the emission bands, the overall white response of the devices lays on the daylight white region – *i.e.*, averaged color correlated temperature of 5500 K – during the whole lifespan (Figure 2). As far as the device performance is concerned, **1**-WLECs stand out compared to other single-component WLECs.[16–19,51] In detail, the average voltage exponentially decreases up to *ca*. 4 V during the first hour due to the formation of the electrical double layers (EDLs) at the electrode interfaces, allowing both charge injection and stabilization of the doped regions. At the same time, the luminance slowly increases reaching a remarkable value of *ca*. 50 cd/m^2 associated to an efficacy of 2.6 cd/A and a lifetime superior to 40 h. Here, the average applied voltage remains fairly constant ($\Delta V<100$ mV), suggesting that the decay of the luminance is likely related to the reduction of the thickness of the emitting p-i-n region.

Small electroluminescence color changes over time can be ascribed to multiple reasons in LECs, namely *i*) unbalanced doping and movement of the emitting p-i-n regions,[1] *ii*) increase of the operation temperature,[52,53] *iii*) changes in the local electric field distribution and intensity,[19,20,54,55] and *iv*) microcavity and scattering effects.[6,56,57] Though the nature of the excited states involved in the mid- and low-energy electroluminescent bands – *i.e.*, λ_{max} of 505 and 695 nm, respectively – is puzzling compared to the blue photoluminescence at room temperature that just matches to the high-energy electroluminescent peak – *i.e.*, λ_{max} = 435 nm. However, this peak slowly despairs, while the mid-energy spectrum evolves into a broad band centered at 530 nm (Figure 2). Compared to the photoluminescence emission in frozen solvent matrix (77 K; Figure S4), the maximum wavelength value of the mid-energy band (530 nm) hints at the presence of a phosphorescence mechanism. This further confirmed in thin film (*vide infra*). However, the well-structured low-energy band, which is the key emissive feature providing high quality white lighting, has not been observed in both photophysical characterizations in solution [25-30,34–44,46–48,] and lighting devices,[31,44,49,50] up to date.

Based on the prior art in both single-component WLECs and WOLEDs,[17–22,51,54,55,58] three hypothesis can be postulated regarding the origin the low-energy emission band, namely *i*) ion-doped matrix-molecule interactions, *ii*) lower-energy emitting degradative species of **1**, and *iii*) exciplex, electromeric, and/or aggregation phenomena. At first, we focused on probing any

interactions between **1** and the ion-doped matrix components. Although the photoluminescence profiles are very similar for pristine films and the active layers (Figure 1), we performed ^{1}H-NMR analysis of **1**, the ion-doped matrix, and mixtures of **1**:ion-doped matrix in solution at increasing concentrations (up to 100 times) of the ion-doped matrix (Figure S5). The high concentration of the matrix resembles a *quasi*-solid-state configuration in which **1** is heavily diluted into the matrix. No noticeable differences in the ^{1}H-NMR spectra were observed, suggesting the absence of any interactions between **1** and the ion-doped matrix. Noteworthy, the absence of dimers or multiple emitting species was also confirmed by performing excitation spectra in the range λ=290-430 nm as well as emission spectra of highly concentrated solutions at high and low temperatures (Figure S2). In addition, preliminary theoretical calculations were performed for single and dimer molecules. While a reasonable agreement with the experimental absorption and the high and mid-energy peak emission spectra was noted, no emission band in the red region (~700 nm) was noted. This might indicate that the nature of this band is not related to a new thermally activated radiative pathway involving a monomer or dimer structure of **1** (*vide infra*). In spite of the degree of agreement found with the experimental results, known limitations of the theoretical methods used for the description of these type of systems (see, for instance, Huang, S.; Zhang, Q.; Shiota, Y.; Nakagawa, T.; Kuwabara, K.; Yoshizawa, K.; Adachi, C. J. Chem. Theory Comput. 2013, 9, 3872−3877 and Hait, D; Zhu, T.; McMahon, D.; Van Voorhis, T J. Chem. Theory Comput. 2016, 12, 3353−3359) cast some doubts on the reliability of the results. Thus, further information has not been provided in the text.

To discard any chemical degradation of **1** upon both device fabrication and operation,[18,19,59,60] we first looked for any relationship between the intensity changes for each band over the whole device lifespan. Figure S6 displays that the intensity of the high-energy peak increases during the first hour until it starts to decay. Unrelatedly, the behavior of both mid- and low-energy bands is similar, showing a slow exponential increase at different rates followed by a slow decrease over time. This indicates that the three bands are independent, and their changes are not related to the formation of degradative species of **1**. Nevertheless, we further compared the spectroscopic features of fresh and used devices (Figure S7). For instance, both absorption and emission spectra are very similar, confirming the lack of new species formed under electrical stimuli. At last, we tackle this study using electrochemical impedance spectroscopy (EIS) to investigate the electrical behavior of fresh and used devices. Under static EIS measurements (Figures 3, S8, and S9), fresh devices show a common LEC behavior, namely *i*) an initial decrease of the electronic resistance at biases below the energy band-gap (*ca*. 3.5-4 V), which corresponds to the formation of the electrical double layer (EDL) formation,

and *ii*) a further resistance decrease that holds at higher biases, which accounts for the formation of the doped regions and the auto-sustained charge recombination (Figure 3). In addition, fresh and used devices showed ionic resistance (σ) values of 1×10^6 Ω and 1×10^5 Ω at 0V, respectively. A decrease of the σ in used devices indicates the lack of degradative events at the electrodes interfaces,[19,59,61] while it is attributed to the remaining polarization upon forming the p- and n-doped regions. Upon heating the used devices at 90 ºC for 30 min, the value of σ is significantly recovered (78% or 0.78×10^6 Ω), indicating that no electrochemical degradation processes are taking place.[19,59,61] In line with the recovery of σ, the shape of the Nyquist plots of fresh devices consists of flattened semicircles, as expected from the poor charge storage capacity and σ values. In contrast, used devices show *quasi*-perfect semicircles due to the polarization effect of the electrochemical doping. After the heating treatment, the Nyquist shape resembles those of fresh devices, indicating that the polarization has been reversibly erased.

Finally, we examine the possible formation of exciplex species at the electrode interfaces,[14,15] aggregates at the active layer,[21] and/or the formation of electromeric emitters.[20,54,55] The exciplex emission was discarded preparing a single-layer device changing the electrodes for bare ITO and Ag (Figure S10). The electroluminescence response corresponds to a white emission as observed for the classical device configuration, showing the same behavior over time with respect to device color – *i.e.*, x/y CIE color coordinates 0.28/0.31 and 0.31/0.38 in concert with CRI values of 89 and 85 at the beginning and the end of the device lifespan, respectively. Noteworthy, these devices also show a high luminance of around 70 cd/m^2 and efficiency of 3.1 cd/A. In line with the above experiments (Figures S5-10), the observed steady electroluminescence behavior further confirms the lack of degradation upon evaporating different metal cathodes.

Aggregated species usually feature either a low efficient and broad emission spectrum or an enhanced emission depending on the type of aggregates and/or aggregated-induced emission takes over.[14,15,62,63] However, the ion-doped matrix has been designed to avoid the formation of aggregates, including a high amount of PS. Indeed, the mixture of **1** and the standard matrix – *i.e.*, **1**:PEO:LiTf in a mass ratio 1:0.15:0.06 – leads to non-homogeneous films with big crystalline-like aggregates and a similar photoluminescence response, but with a strongly reduced ϕ compared to that measured for pristine films and device active layers (Figure S11). Indeed, these devices did not show any electroluminescence response, indicating that the presence of crystalline-like aggregates are effective emission quenchers in **1**. The presence of crystalline-like aggregates disrupts the homogeneity of the thin film, leading to the formation

of shorts whenever the device is run. Finally, the low-energy band in the electroluminescence spectrum shows a well-defined structure with a maximum at 695 nm and a shoulder at 750 nm; features that are not expected from an emission originated from aggregates.

The formation of electromeric emitting species is related to the presence of a pair of statistically independent **1** molecules, combining an ionic and cationic forms – *i.e.*, ($\mathbf{1}^{-}$/$\mathbf{1}^{+}$)* singlet or triplet states – under the presence of high electric fields. Similar to the exciplex- and aggregated-like electroluminescence, they are sensitive to the emitter concentration, but even more to the externally applied electric field.[20,54,55] Thus, we decided to prepare a new set of devices increasing the amount of PS and thickness to further avoid the presence of any aggregate species and to significantly reduce the built-up electric field at the active layer – *i.e.*, ITO/PEDOT:PSS(70 nm)/**1**:PS:PEO:LiOTf 10:1.8:2.6:0.78(100 nm)/Al(90nm). In addition, these devices were driven at 9V pulsed voltage to study if the driving operation has any effect on the electroluminescence behavior. As shown in Figure 4, the electrical device behavior is common for all LECs – *vide supra*, while the white response is preserved showing a broad band with maxima at 435, 560, 690, and 750 nm. The initial emission corresponds to x/y CIE color coordinates of 0.29/0.35 and CRI of 87, which quickly change to 0.33/0.38 and CRI of 85 after 30 seconds, remaining constant throughout the lifespan of the device. In addition, these devices also show good luminance levels of *ca*. 30 cd/m^2, efficiency of 2.5 cd/A, and stabilities over days. As such, the white response and device performance hold regardless the device architecture – *i.e.*, active layer composition, thickness, and type of electrodes – as well as the driving modes, excluding all of the known reasons to reveal the nature of the low-energy emitting band.

A remaining aspect long overlooked in LECs is the heat generation under operation conditions. Indeed, **1**-WLECs feature an increase of the pixel temperature between 45-65 ºC holding constant during the measurements (Figure S12). Thus, we decided to investigate the temperature dependence of the photoluminescence of **1** films. Surprisingly, two new well-structured bands centered at 530 and 700 nm evolved upon heating, leading to a whitish photoluminescence spectrum that is very similar to that observed in all the above described devices (Figure 5). This experiment is indeed crucial as it allowed to correlate the unexpected electroluminescence response with the photoluminescence features, indicating the same radiative mechanism is operative regardless of the excitation way. To elucidate the nature of these emitting excited states, the τ values were determined at 400 nm, 525 nm, and 700 nm corresponding to 3.2 ns, 5.8 μs, and 12.3 μs (Figure S13). Please note that the emission related

to the mid- and low-energy bands is strongly quenched in air even at the high temperature of 400 K (Figure S14), highlighting its sensitivity towards oxygen and suggesting a triplet-based emission. This points out a unique multi-emissive mechanism involving fluorescence at high-energies and thermally activated dual phosphorescence at the mid- and low-energy parts of the visible spectrum. These findings are also valid for the temperature dependence photoluminescence of **1** devices. Notably, the film morphology (Figure S15) and the above τ values (Table S1) of **1** devices are not affected upon heating for long periods of time – *i.e.*, 60 ºC for 7 days. These findings allow us to discard long range changes of the chemical and structural surrounding of **1**, as well as effects of the substrates. In addition, the theoretical description of the manifold of excited states of **1** and its related dimmers discards that the low-emission band is a figure for the BN doping pattern of **1**. Therefore, we conclude that the low emission must be related to temperature-induced short-range molecular and/or domain conformations in thin-films. Further studies using transient spectroscopy coupled to both temperature and electric fields are on-going in our laboratories.

As Figure 5 displays, the ternary white emission might be even more prominent in devices, as the spin statistics upon charge recombination promotes the formation of triplets (75%) over singlets (25%). Differences in the device temperature and the statistics formation rate of mid- and low-energy emitting triplets under different electric fields could explain the discrepancies between the intensity peaks upon comparing both photo- and electro-electroluminescence responses (Figure 5), as well as the electroluminescence spectra between devices with different architectures and driving conditions (Figures 2, 4, and 5). For instance, thick devices driven at pulsed voltage featured 65 ºC, exhibiting a very small high-energy intensity and a well-balanced emission intensity between the mid- and low-energy bands, while thin devices operating at pulsed current reached 40 ºC, showing a more prominent high-energy band and less intense low-energy bands. Please note that the previously commented time-dependent redshift of the low-energy electroluminescence peak was ascribed to the rise in temperature upon device driving, which takes place in the first stage of device operation (Figure S12).

3. Conclusions

This work presents one of the most outstanding performances in single-component SM-WLECs, encompassing white color (average x/y CIE color coordinates of 0.28-31/0.31-0.38 and CRI of 87), luminance values around 50-70 cd/m^2, efficiencies of *ca*. 3 cd/A, and stabilities of days. This has been realized applying, for the first time, BN-doped nanographenes with the

B_3N_3 doping pattern as single emitters. After having discarded prior reported reasons for a white electroluminescence using non-white-emitting compounds in single-component WLECs and WOLEDs – *i.e.*, device architecture, driving conditions, presence of degradative and aggregated species, as well as excimeric and electromeric emissions –, we have concluded that the origin of the white electroluminescent response is a unique ternary emission mechanism involving a fluorescence and a thermally-activated dual phosphorescence that can be seen as a frustrated TADF mechanism.

The relevance of this finding is clearly stated by three facts. First, the presence of ternary photoluminescence in engineered emitters has just been announced,[23] while this work presents the first example rationalizing how the B_3N_3 doping pattern in BN-doped nanographenes leads to a highly desired white multi-emissive photo- and electro-luminescence responses. Second, this exclusive ternary emission mechanism leads to one of the best performing thin-film white-emitting devices compared to the prior-art. Third, this contribution sheds light onto the prospect of the BN doping approach to design new functional nanographenes with tailored photo- and electro-luminescent features. In particular, we highlight, for the first time, that the replacement of the C=C bonds with B=N couples in a B_3N_3 fashion is a powerful approach to design white-emitting nanographenes for efficient single-component white-emitting devices. Other groups like Bettinger, Bragg,[28–30] Piers,[32] Hatakeyama[31,44] have also provided excellent examples about the effect of the B-N doping pattern on the emission features, showing several examples of high-energy TADF emission.

Overall, the designing principle to program BN-doped molecular graphenes is still in its infancy, opening new horizons in using this doping approach for the preparation of functional nanographenes with tailored photo- and electro-luminescent properties. As shown in this work, this family of compounds exhibit, in addition, an interesting photoluminescence behavior in thin films with regards to externally applied temperature and electric field. A solid understanding of the emission mechanism in thin films under the above conditions is still highly desired. Transient spectroscopy coupled to both temperature and electric fields is on-going in our laboratories. These aspects represent the challenge of our forthcoming activities in the field of molecular BN-doped materials towards realizing highly efficient and stable single-component and single-layered white-emitting devices.

Supporting Information
Supporting Information is available from the Wiley Online Library or from the author.

Acknowledgements

E.F. and R.D.C. acknowledge the program "Ayudas para la atracción de talento investigador - Modalidad 1 of the Consejería de Educación, Juventud y Deporte—Comunidad de Madrid with the Reference No. 2016-T1/IND- 1463.". R.D.C. also acknowledges the Spanish MINECO for the Ramón y Cajal program (RYC-2016-20891), the Europa Excelencia program (ERC2019- 092825), and HYNANOSC (RTI2018-099504-A-C22), as well as the 2018 Leonardo Grant for Researchers and Cultural Creators from BBVA Foundation and the FOTOART-CM project funded by Madrid region under programme P2018/NMT-4367. D.B. and J.D. gratefully acknowledge the EU through the MC-RISE project 'INFUSION' and Cardiff University for the financial support. J. F-C acknowledge the Marie Skłodowska-Curie Individual Fellowships (H2020-MSCA-IF-2017). The authors heartily thanks Pedro B. Coto was his efforts on the theoretical characterization of **1**.

4. References

[1] S. Tang, A. Sandström, P. Lundberg, T. Lanz, C. Larsen, S. Van Reenen, M. Kemerink, L. Edman, *Nat. Commun.* **2017**, *8*, 1190.

[2] Z. Zhang, Y. Li, G. Guan, H. Li, Y. Luo, F. Zhao, Q. Zhang, B. Wei, Q. Pei, H. Peng, Z. Zhang, K. Guo, Y. Li, X. Li, G. Guan, H. Li, Y. Luo, F. Zhao, Q. Zhang, B. Wei, Q. Pei, H. Peng, *Nat. Photonics* **2015**, *9*, 233.

[3] A. Sandstroem, A. Asadpoordarvish, J. Enevold, L. Edman, *Adv. Mater.* **2014**, *26*, 4975.

[4] G. Hernandez-Sosa, S. Tekoglu, S. Stolz, R. Eckstein, C. Teusch, J. Trapp, U. Lemmer, M. Hamburger, N. Mechau, *Adv. Mater.* **2014**, *26*, 3235.

[5] A. Asadpoordarvish, A. Sandström, C. Larsen, R. Bollström, M. Toivakka, R. Österbacka, L. Edman, *Adv. Funct. Mater.* **2015**, *25*, 3238.

[6] H.-C. Su, C.-Y. Cheng, *Isr. J. Chem.* **2014**, *54*, 855.

[7] E. Fresta, R. D. Costa, *J. Mater. Chem. C* **2017**, *5*, 5643.

[8] R. D. Costa, *Light-emitting electrochemical cells. Concepts, advances and challenges.*; 1st ed.; Springer International Publishing: Basel, 2017.

[9] H. C. Su, H. F. Chen, F. C. Fang, C. C. Liu, C. C. Wu, K. T. Wong, Y. H. Liu, S. M. Peng, *J. Am. Chem. Soc.* **2008**, *130*, 3413.

[10] L. He, J. Qiao, L. Duan, G. Dong, D. Zhang, L. Wang, Y. Qiu, *Adv. Funct. Mater.* **2009**, *19*, 2950.

[11] M. L. Wu, G. Y. Chen, T. A. Shih, C. W. Lu, H. C. Su, *Phys. Chem. Chem. Phys.* **2018**, *20*, 18226.

[12] G.-R. Lin, J.-R. Cheng, C.-W. Wang, M. Sarma, H.-F. Chen, H.-C. Su, C.-H. Chang, K.-T. Wong, *J. Mater. Chem. C* **2015**, *3*, 12492.

[13] T. Akatsuka, C. Roldán-Carmona, E. Ortí, H. J. Bolink, *Adv. Mater.* **2014**, *26*, 770.

[14] Y. Nishikitani, H. Takeuchi, H. Nishide, S. Uchida, S. Yazaki, S. Nishimura, *J. Appl. Phys.* **2015**, *118*.

[15] S. Uchida, D. Takizawa, S. Ikeda, H. Takeuchi, S. Nishimura, H. Nishide, Y. Nishikitani, *J Vis Exp* **2016**, *117*, e54628.

[16] Y. Yang, Q. Pei, *J. Appl. Phys.* **1997**, *81*, 3294.

[17] S. Tang, J. Pan, H. a Buchholz, L. Edman, *J. Am. Chem. Soc.* **2013**, *135*, 3647.

[18] M. D. Weber, M. Adam, R. R. Tykwinski, R. D. Costa, *Adv. Funct. Mater.* **2015**, *25*, 5066.

[19] M. D. Weber, J. E. Wittmann, A. Burger, O. B. Malcioglu, J. Segarra-Martínez, A. Hirsch, P. B. Coto, M. Bockstedte, R. D. Costa, *Adv. Funct. Mater.* **2016**, *26*, 6737.

[20] J. Y. Li, D. Liu, C. Ma, O. Lengyel, C. S. Lee, C. H. Tung, S. Lee, *Adv. Mater.* **2004**, *16*, 1538.

[21] M. Mazzeo, V. Vitale, F. Della Sala, M. Anni, G. Barbarella, L. Favaretto, G. Sotgiu, R. Cingolani, G. Gigli, *Adv. Mater.* **2005**, *17*, 34.

[22] S. Park, J. E. Kwon, S. H. Kim, J. Seo, K. Chung, S.-Y. Park, D.-J. Jang, B. M. Medina, J. Gierschner, S. Y. Park, *J. Am. Chem. Soc.* **2009**, *131*, 14043.

[23] C. Zhou, S. Zhang, Y. Gao, H. Liu, T. Shan, X. Liang, B. Yang, Y. Ma, *Adv. Funct. Mater.* **2018**, *28*, 1802407.

[24] J. Dosso, J. Tasseroul, F. Fasano, D. Marinelli, N. Biot, A. Fermi, D. Bonifazi, *Angew. Chem., Int. Ed.* **2017**, *56*, 4483.

[25] Z. X. Giustra, S. Y. Liu, *J. Am. Chem. Soc.* **2018**, *140*, 1184.

[26] X. Y. Wang, J. Y. Wang, J. Pei, *Chem. - A Eur. J.* **2015**, *21*, 3528.

[27] D. Bonifazi, F. Fasano, M. M. Lorenzo-Garcia, D. Marinelli, H. Oubaha, J. Tasseroul, *Chem. Commun.* **2015**, *51*, 15222.

[28] J. A. Snyder, P. Grüninger, H. F. Bettinger, A. E. Bragg, *J. Phys. Chem. A* **2017**, *121*, 5136.

[29] J. A. Snyder, P. Grüninger, H. F. Bettinger, A. E. Bragg, *J. Phys. Chem. A* **2017**, *121*, 8359.

[30] S. A. Brough, A. N. Lamm, S. Y. Liu, H. F. Bettinger, *Angew. Chem. Int. Ed.* **2012**, *51*,

10880.

[31] K. Matsui, S. Oda, K. Yoshiura, K. Nakajima, N. Yasuda, T. Hatakeyama, *J. Am. Chem. Soc.* **2017**, *140*, 1195.

[32] M. J. D. Bosdet, W. E. Piers, T. S. Sorensen, M. Parvez, *Angew. Chem. Int. Ed.* **2007**, *46*, 4940.

[33] A. Abengózar, P. García-García, D. Sucunza, A. Pérez-Redondo, J. J. Vaquero, *Chem. Commun.* **2018**, *54*, 2467.

[34] M. M. Lorenzo-García, D. Bonifazi, *Chim. Int. J. Chem.* **2017**, *71*, 550.

[35] L. Brown, C.-J. Kim, R. W. Havener, D. A. Muller, P. Y. Huang, J. Park, M. P. Levendorf, *Nature* **2012**, *488*, 627.

[36] P. M. Ajayan, S. Lei, A. Babakhani, X. Yang, W. Zhou, K. P. Hackenberg, J. Zhang, Y. Gong, J.-C. Idrobo, Z. Liu, R. Vajtai, G. Shi, J. Lou, L. Ma, J. Yu, *Nat. Nanotechnol.* **2013**, *8*, 119.

[37] M. Krieg, F. Reicherter, P. Haiss, M. Ströbele, K. Eichele, M. J. Treanor, R. Schaub, H. F. Bettinger, *Angew. Chem. Int. Ed.* **2015**, *54*, 8284.

[38] Z. Liu, T. B. Marder, *Angew. Chem. Int. Ed.* **2008**, *47*, 242.

[39] H. Helten, *Chem. - A Eur. J.* **2016**, *22*, 12972.

[40] X. Chen, H. Yang, B. Wu, L. Wang, Q. Fu, Y. Liu, *Adv. Mater.* **2019**, *31*, 1805582.

[41] M. Fan, J. Wu, J. Yuan, L. Deng, N. Zhong, L. He, J. Cui, Z. Wang, S. K. Behera, C. Zhang, J. Lai, B. M. I. Jawdat, R. Vajtai, P. Deb, Y. Huang, J. Qian, J. Yang, J. M. Tour, J. Lou, C. W. Chu, D. Sun, P. M. Ajayan, *Adv. Mater.* **2019**, *31*, 1805778.

[42] U. Hahn, E. Maisonhaute, J. F. Nierengarten, *Angew. Chem. Int. Ed.* **2018**, *57*, 10635.

[43] X. Y. Wang, A. Narita, X. Feng, K. Müllen, *J. Am. Chem. Soc.* **2015**, *137*, 7668.

[44] S. Nakatsuka, T. Hatakeyama, T. Ikuta, K. Kinoshita, S. Nomura, Y. Ono, J. Ni, K. Nakajima, K. Shiren, *Adv. Mater.* **2016**, *28*, 2777.

[45] D. Portehault, D. Liu, Y. Chen, S. Qin, J. Hao, J. Wang, Y. Li, W. Lei, *ACS Energy Lett.* **2017**, *2*, 306.

[46] A. M. Abdalla, S. Hossain, O. B. Nisfindy, A. T. Azad, M. Dawood, A. K. Azad, *Energy Convers. Manag.* **2018**, *165*, 602.

[47] B. Li, Z. Liu, M. Vasiliu, A. Chrostowska, S.-Y. Liu, J. S. A. Ishibashi, A. Dargelos, D. A. Dixon, C. Darrigan, *J. Am. Chem. Soc.* **2017**, *139*, 6082.

[48] J. Y. Wang, J. Pei, *Chinese Chem. Lett.* **2016**, *27*, 1139.

[49] S. Nakatsuka, N. Yasuda, T. Hatakeyama, *J. Am. Chem. Soc.* **2018**, *140*, 13562.

[50] S. Kervyn, O. Fenwick, F. Di Stasio, Y. S. Shin, J. Wouters, G. Accorsi, S. Osella, D.

Beljonne, F. Cacialli, D. Bonifazi, *Chem. - A Eur. J.* **2013**, *19*, 7771.

[51] S. Tang, J. Pan, H. Buchholz, L. Edman, *ACS Appl. Mater. Interfaces* **2011**, *3*, 3384.

[52] D. Asil, J. A. Foster, A. Patra, X. Dehatten, J. Delbarrio, O. A. Scherman, J. R. Nitschke, R. H. Friend, *Angew. Chem. Int. Ed.* **2014**, *53*, 8388.

[53] M. H. Bowler, T. Guo, L. Bastatas, M. D. Moore, A. V Malko, J. D. Slinker, *Mater. Horiz.* **2017**, *4*, 657.

[54] H. Yu, Y. Zhang, Y. J. Cho, H. Aziz, *ACS Appl. Mater. Interfaces* **2017**, *9*, 14145.

[55] Y. J. Cho, S. Taylor, H. Aziz, *ACS Appl. Mater. Interfaces* **2017**, *9*, 40564.

[56] G. R. Lin, H. R. Chen, H. C. Shih, J. H. Hsu, Y. Chang, C. H. Chiu, C. Y. Cheng, Y. S. Yeh, H. C. Su, K. T. Wong, *Phys. Chem. Chem. Phys.* **2015**, *17*, 6956.

[57] N. Kaihovirta, C. Larsen, L. Edman, *ACS Appl. Mater. Interfaces* **2014**, *6*, 2940.

[58] G. M. Farinola, R. Ragni, *Chem. Soc. Rev.* **2011**, *40*, 3467.

[59] M. D. Weber, E. Fresta, M. Elie, M. E. Miehlich, J.-L. Renaud, K. Meyer, S. Gaillard, R. D. Costa, *Adv. Funct. Mater.* **2018**, *28*, 1707423.

[60] E. Fresta, J.-M. Carbonell-Vilar, J. Yu, D. Armentano, J. Cano, M. Viciano-Chumillas, R. D. Costa, *Adv. Funct. Mater.* **2019**, *29*, 1901797.

[61] L. D. Bastatas, K. Y. Lin, M. D. Moore, K. J. Suhr, M. H. Bowler, Y. Shen, B. J. Holliday, J. D. Slinker, *Langmuir* **2016**, *32*, 9468.

[62] E. Fresta, G. Volpi, C. Garino, C. Barolo, R. D. Costa, *Polyhedron* **2018**, *140*, 129.

[63] J. Mei, N. L. C. Leung, R. T. K. Kwok, J. W. Y. Lam, B. Z. Tang, *Chem. Rev.* **2015**, *115*, 11718.

[64] C. M. Luk, L. B. Tang, W. F. Zhang, S. F. Yu, K. S. Teng, S. P. Lau, *J. Mater. Chem.* **2012**, *22*, 22378.

Figures

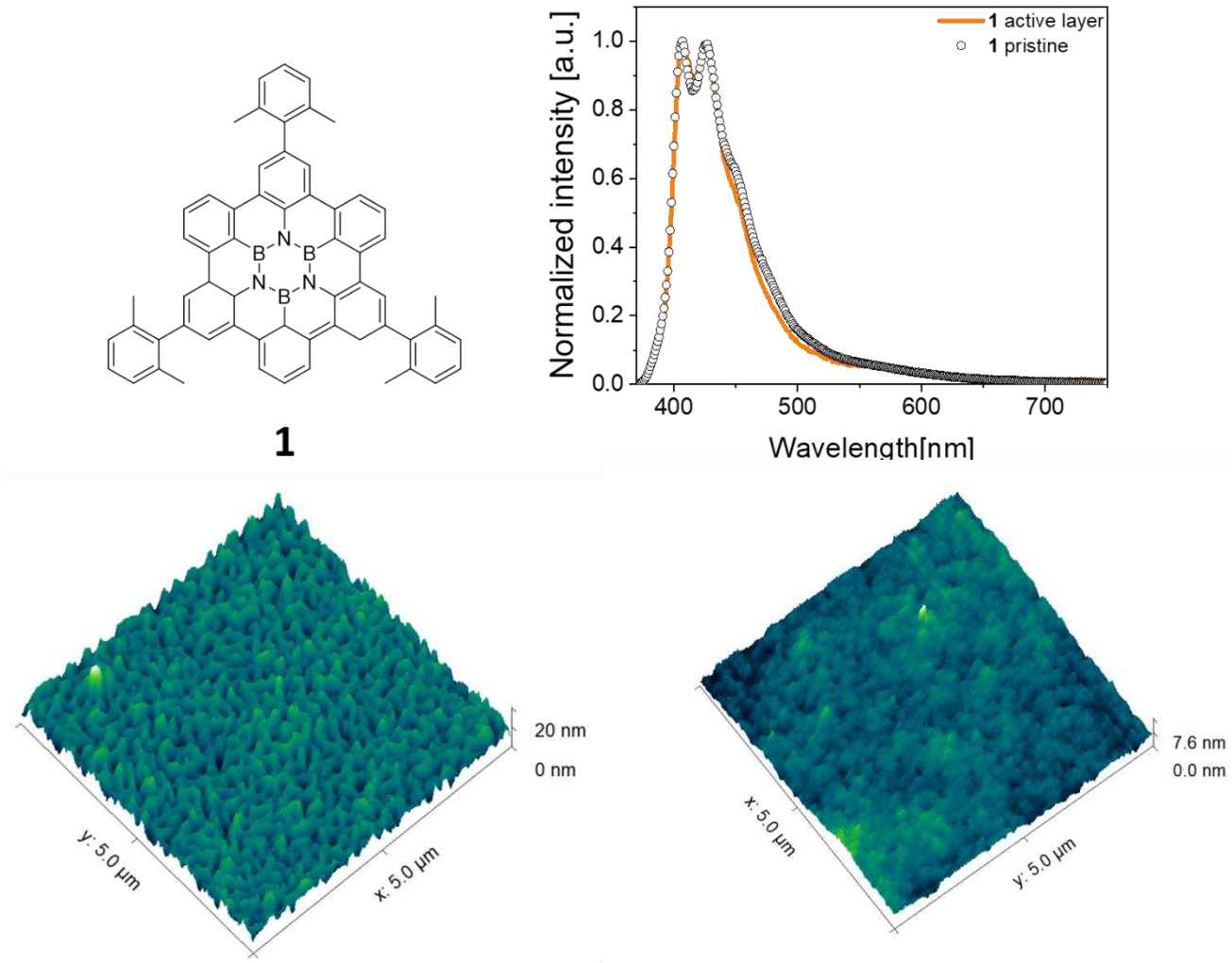

Figure 1. Top, left: Chemical structure of **1**. Top, right: Photoluminescence spectra (λ_{exc} = 355 nm) of thin-films based on **1** with (active layer) and without (pristine) ionic matrix onto ITO/PEDOT:PSS substrates in air at room temperature. Inset: Table summarizing the photoluminescence figures-of-merit, namely ϕ and τ. Bottom: AFM pictures of thin films based on **1** with (active layer; left) and without ionic matrix (pristine; right).

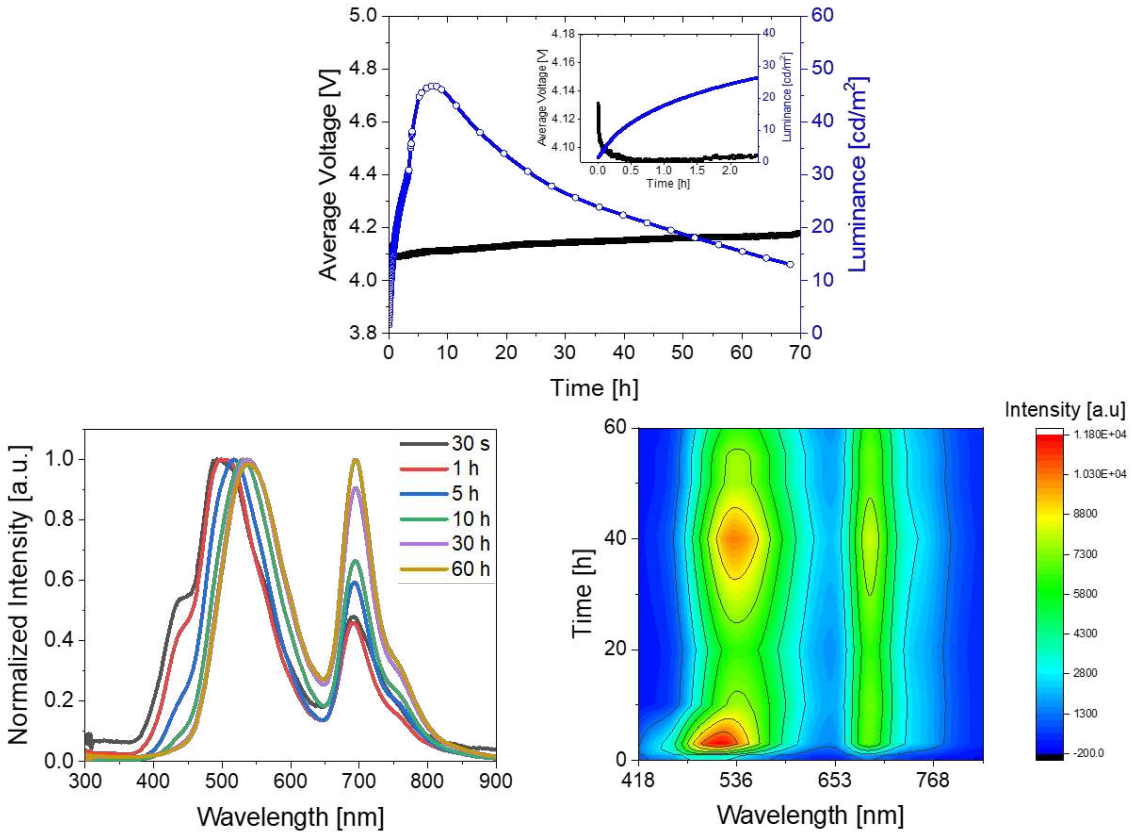

Figure 2. Top: Luminance and applied voltage over time of thin **1**-WLECs driven at pulsed 5 mA. The inset graph highlights the device behavior during the first 2 hours. Bottom: Electroluminescence changes over time highlighted by representative spectra (left) taken at different times (see legend) and 2D electroluminescence map evolution (right).

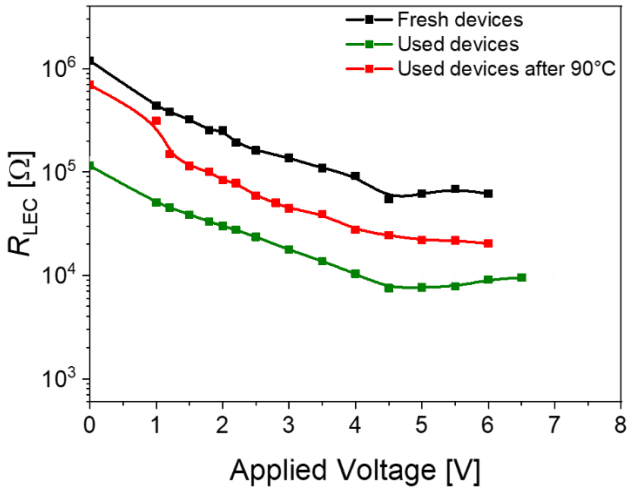

Figure 3. Static EIS assays applied to **1**-WLECs to monitor the changes of the device behavior of fresh, used, and after heating at 90 ºC devices with respect to the resistance values associated to the EDL and doped region formations upon increasing the applied voltage from 0 to 6 V.

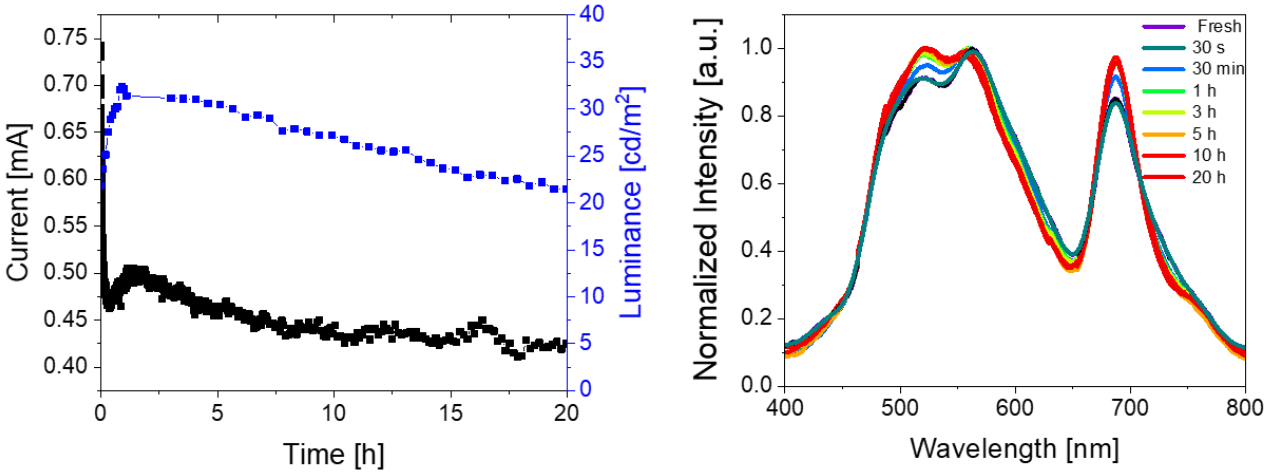

Figure 4. Left: Luminance and applied voltage over time of thick **1**-WLECs driven at pulsed 9 V. Right: Electroluminescence changes over time highlighted by representative spectra taken at different times (see legend).

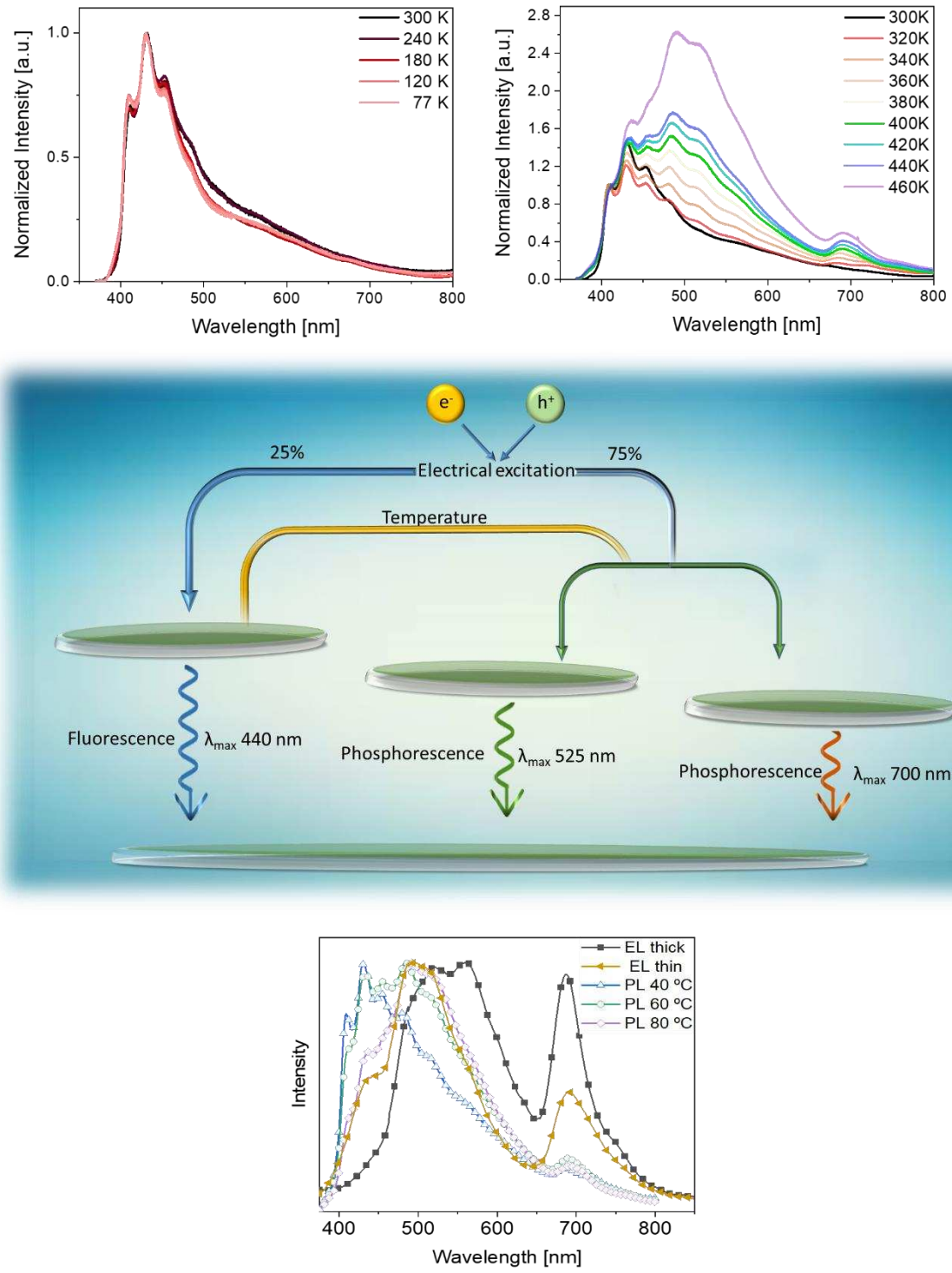

Figure 5. Top: Photoluminescence spectra (λ_{exc}=355 nm) of **1** films on quartz upon heating from 77 K to 300 K (left) and from 300 K to 460 K (right). Middle: Sketch highlighting the ternary electroluminescence mechanism involving fluorescence and thermally activated dual phosphorescence. Bottom: Comparison of the photoluminescence spectra (open symbols) of **1** thin films at different temperatures (see legend) and the electroluminescence spectra (full symbols) of both thin and thick **1**-WLECs.

Table of Content

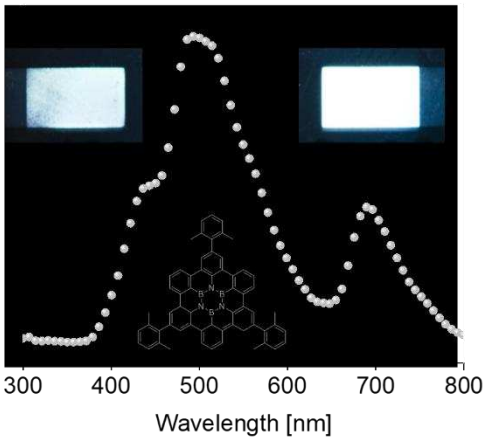

Supporting Information

Origin of the exclusive ternary electroluminescent behavior of BN-doped nanographenes in efficient single-component white light-emitting electrochemical cells

Elisa Fresta, Jacopo Dosso, Juan Cabanillas-González, Julio Fernandez-Cestau, Davide Bonifazi, and Rubén D. Costa*

Elisa Fresta, Julio Fernandez-Cestau and Dr. Rubén D. Costa*
IMDEA Materials Institute, Calle Eric Kandel 2, E-28906 Getafe, Madrid, Spain.
ruben.costa@imdea.org

Elisa Fresta
Universidad Autónoma de Madrid, Departamento de Física Aplicada, Calle Francisco Tomás y Valiente, 7, 28049 Madrid, Spain.

Jacopo Dosso and Prof. Davide Bonifazi
School of Chemistry, Cardiff University, CF10 3AT Cardiff, Great Britain.

Dr. Juan Cabanillas
IMDEA Nanoscience, Calle Faraday 9, 28049 Madrid, Spain.

Outline

1. Experimental

Materials

All chemicals were purchased from chemical suppliers and used without further purification. All analytical reagent grade solvents were purified by distillation. All reactions were carried out under inert nitrogen atmosphere using standard vacuum lines techniques. Deuterated solvents were purchased from Eurisotop and Sigma Aldrich.

Synthesis, spectroscopic, and microscopy characterization

1 was synthesized as reported in a previous contribution.[1] Its purification was carried out using two consecutive SCC (size exclusion chromatography) (eluent: Petroleum ether/CH_2Cl_2 8/2). When recycling HPLC was performed, it was necessary to use a Petroleum Ether/CH_2Cl_2 6/4 eluent due to solubility issues in order to avoid precipitation in the column. To further purify the desired product, three consecutive preparative TLCs (thin layer chromatography) with petroleum ether/CH_2Cl_2 8/2 as eluent were carried out, allowing for the obtainment of **1** as a clean product. Excitation emission analyses were then performed to exclude the presence of other emissive species (Figure S2). This was done in combination with ^{1}H-NMR experiments (Figure S3). Please note that a clear correspondence between the absorption and emission peaks (within experimental error of ± 2 nm) can be noticed from the excitation envelope. (e.g., Absorption: 314 nm, 335 nm, 354 nm, 373 nm; Emission: 383 nm, 404 nm (max), 426 nm, 452 nm. This confirms that **1** is the only emitting specie.

Absorption spectra were recorded with a Perkin Elmer Lambda 35 UV-Vis spectrometer. The photoluminescence spectra and photoluminescence quantum yield values were measured with a FS5 Spectrofluorometer with integrating sphere SC-30 (Edinburgh Instruments). Thin films (75 nm) were prepared onto cleaned quartz slides from a filtered solution of **1** (15 mg/mL in THF; without ion-doped matrix or with as below described) by spin-coating them at 800 rpm for 30 s, at 1500 rpm for 30 s and at 3000 rpm for an additional 10 s. Excited states lifetimes of fluorescence emission were obtained with a TCSPC laser (λ_{exc} 377.6 nm), while the phosphorescence lifetimes at 550 nm and 700 nm were carried with a microsecond lamp using phosphorescence mode with a delay of 1.6 μs. The average lifetime can be obtained by using the $< \tau > = \frac{A_1\tau_1^2+A_2\tau_2^2}{A_1\tau_1+A_2\tau_2}$ formula reported in literature.[64]

Photoluminescence measurements at temperatures ranging from 77 K to 475 K were performed upon enclosing **1** films in a CFV-Optistat (Oxford Instruments) equipped with a temperature controller. Films were photoexcited with a TEEM Photonics passive Q-switch Nd:YAG laser (405 nm, 300 ps pulse duration, 170 Hz, pulse energy < 1 mJ) mildly focused on the sample (fluence < 10 mJ/cm^2). The photoluminescence emitted by the samples was dispersed by a grating inside a spectrometer (SP2500, Acton Research) and spectrally recorded with a liquid N_2-cooled back depleted CCD (Princeton Instruments). Long pass filters were employed to reject stray light from the photoexcitation beam into the spectrometer. The photoluminescence spectra were acquired 10 minutes after the sample reached the desired temperature in order to ensure complete sample thermalization.

^{1}H NMR spectra were recorded on a Bruker Fourier 300 MHz spectrometer equipped with a dual (^{13}C, ^{1}H) probe. ^{1}H spectra were obtained at 300 MHz. All spectra were obtained at rt if not otherwise stated. Chemical shifts were reported in ppm according to tetramethylsilane using the solvent residual signal as an internal reference ($CDCl_3$: δ_H = 7.26 ppm, THF-*d*8: δ_H = 3.58, 1.73 ppm). Coupling constants (*J*) were given in Hz. Resonance multiplicity was described as *s* (singlet), *d* (doublet), *t* (triplet), *dd* (doublet of doublets), *dt* (doublet of triplets), *td* (triplet of doublets), *q* (quartet), *m* (multiplet) and *bs* (broad signal).

AFM measurements were carried out with a Park XE150 instrument (Park Systems Corp., Suwon, South Korea), and the Gwyddion evaluation software.

Device fabrication and characterization

ITO substrates were purchased from Naranjo Substrates with an ITO thickness of 130 nm. They were extensively cleaned using detergent, water, ethanol, and propan-2-ol as solvents in an ultrasonic bath (frequency 37-70 Hz) for 15 min each. Afterwards, the slides were dried with N_2 gas and put in an UV-ozone cleaner for 8 min and used directly as described in the main text. If PEDOT:PSS is used to increase reproducibility, the clean plates were coated with 70 nm PEDOT:PSS layers via spin coating. To this end, an aqueous solution of PEDOT:PSS was filtered and mixed with propan-2-ol in a ratio of 3:1. From this solution, 50 µL were dropped onto the substrate at a rotation speed of 2000 rpm and spun for 60 s. The resulting layers were dried on a hotplate at 120 °C and stored under N_2. Thick active layers (100 nm) were deposited from a 15 mg/mL of **1** combined with a ion-doped matrix consisting of **1**:PS:PEO:LiOTf 10:1.81:2.6:0.78 mass ratio. This was prepared using THF solutions of PS with M_w 900,000 (10 mg/mL), PEO with M_w 8,000,000 (20 mg/mL) and LiOTf (10 mg/ml) and spin coated at 800 rpm for 30 s, at 1500 rpm for 30 s and at 3000 rpm for an additional 10 s, resulting in 100 nm

of active layer thickness. The thin active layers (70 nm) were achieved by employing a ratio **1**:PS:PEO:LiOTf 10:0.9:2.6:0.78 mass ratio, following the same procedure as above. In all cases, after the deposition of the active layer the devices were dried under vacuum for 2 h and transferred to an inert atmosphere glovebox (<0.1 ppm O_2 and H_2O, Angstrom Engineering). Finally, either Aluminum or Silver cathodes (90 nm) were thermally evaporated onto the active layer using a shadow mask under high vacuum (<1 x 10^{-6} mbar) in an Angstrom Covap evaporator integrated into the inert atmosphere glovebox. The device statistics involve up to five different devices – *i.e.*, a total number of 20 pixels. Time dependence of luminance, voltage, and current was measured by applying constant and/or pulsed voltage and current by monitoring the desired parameters simultaneously by using Avantes spectrophotometer (Avaspec-ULS2048L-USB2) in conjunction with a calibrated integrated sphere Avasphere 30-Irrad and Botest OLT OLED Lifetime-Test System. Electroluminescence spectra were recorded using the above mentioned spectrophotometer. Electrochemical impedance spectroscopic assays (EIS) were carried out with a potentiostat/galvanostat (Metrohm μAutolabIII) equipped with a frequency response analyser module (FRA2). Measurements were performed at the applied voltage range from 0 to 6 V and fitted with the Nova software using the circuit model shown in Figure S8. The AC signal amplitude was set to 10 mV, modulated in a frequency range from 10 to 1 MHz. The Nova 1.11 software was used to obtain the parameters from the equivalent circuit. With this data at hand, the resistance of the intrinsic non-doped region (R_{LEC}) was directly obtained. The film conductivity (S/m) is measured at 0 V with the following equation: $\sigma = d/(AR_{LEC})$, where d is the thickness of the layer, A is the area of the electrodes, and R_{LEC} is the resistance of the active layer. The temperature of the devices upon driving was recorded with a FLIR 430-sc thermal camera.

2. Figures

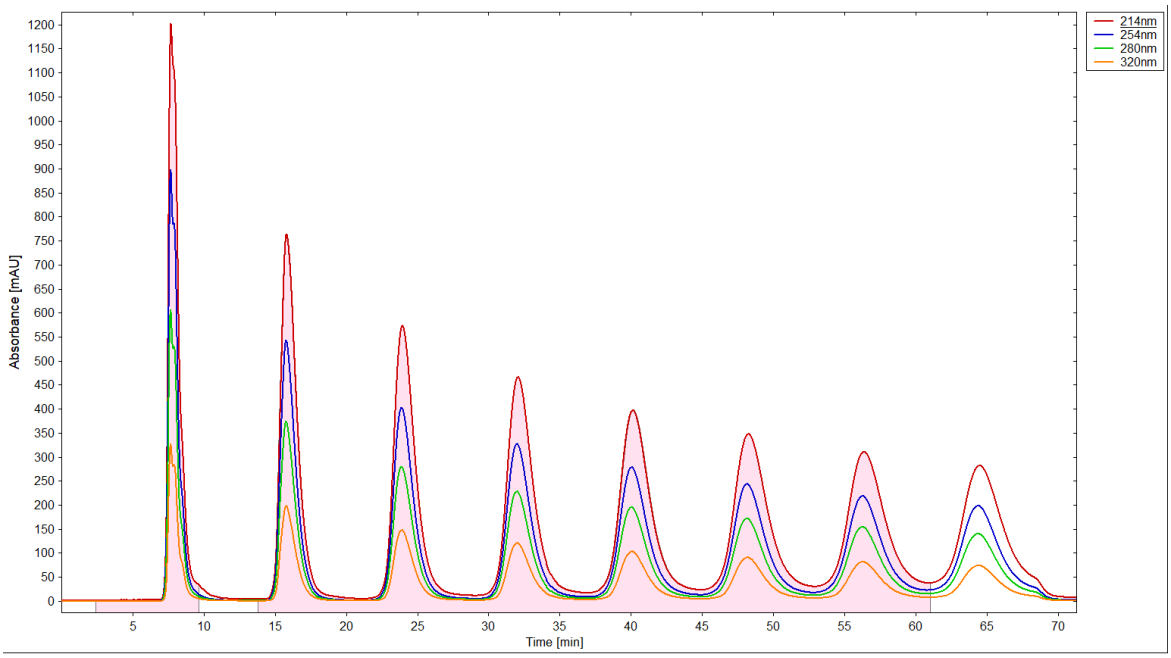

Figure S1. Absorption intensity *versus* retention times for **1** under recycling HPLC with petroleum ether/CH_2Cl_2 6/4 as eluent. The detector wavelengths are reported in the legend.

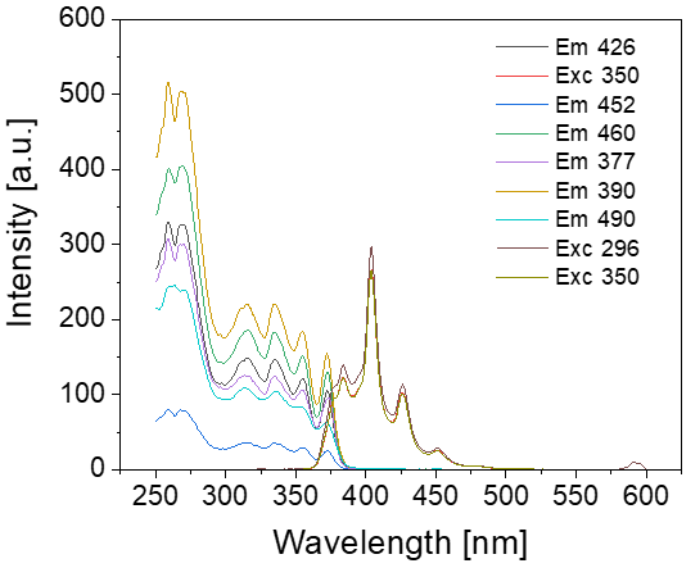

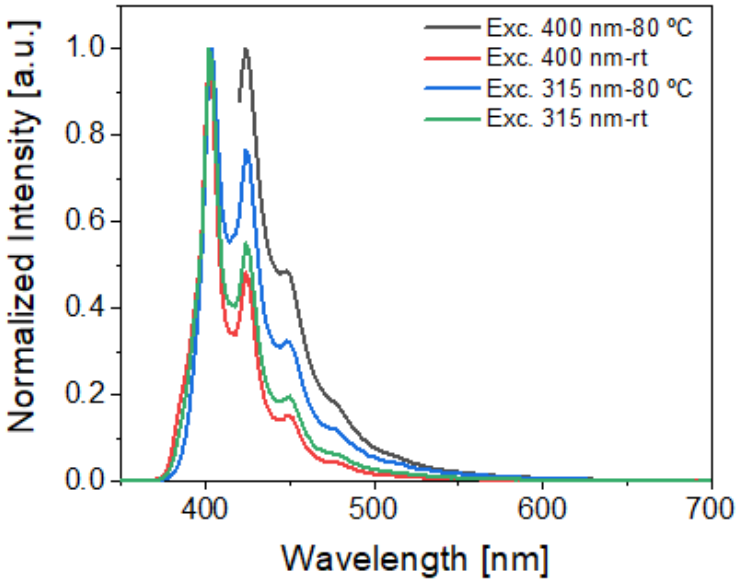

Figure S2. Top: Excitation-emission spectra of **1** recorded in CH_2Cl_2 at rt. The various emission (Em) and excitation (Exc) wavelengths (in nm) are reported in the legend. Bottom: Emission spectra at various excitation wavelengths of **1** in degassed chlorobenzene recorded at rt and 80 °C (see legend).

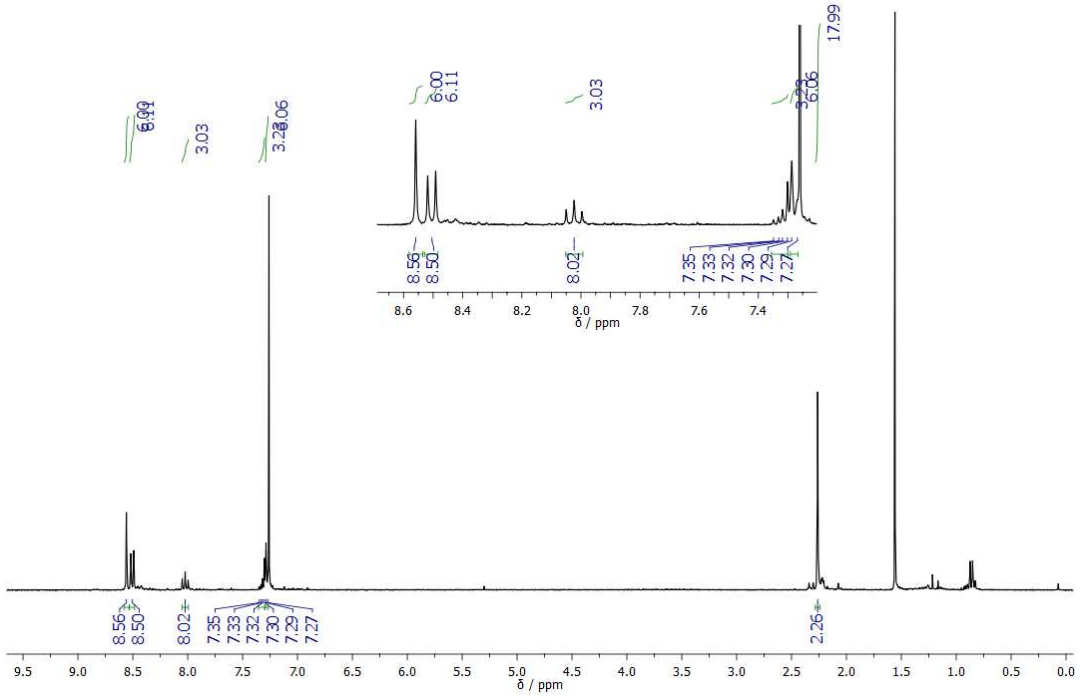

Figure S3. ^{1}H-NMR (300 MHz) of **1** in $CDCl_3$.

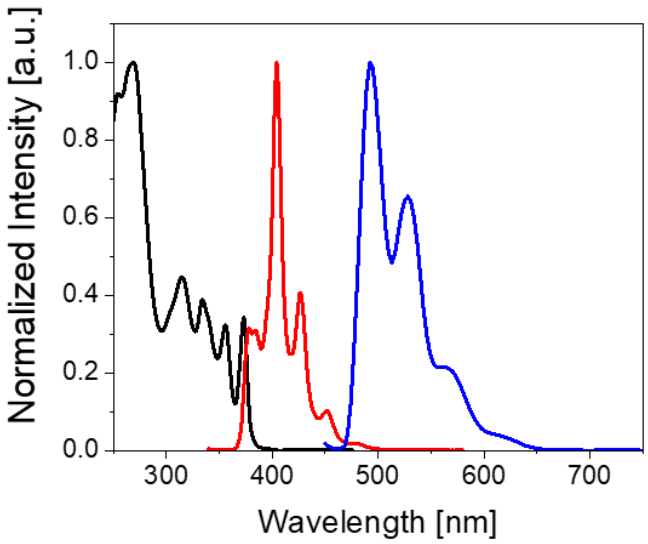

Figure S4. Normalized absorption (black; in air equilibrated CH_2Cl_2 at rt), fluorescence (red; λ_{exc}=315 nm in air equilibrated CH_2Cl_2 at rt), and phosphorescence (blue; λ_{exc}=315 nm at 77 K in a 1:1, v/v CH_2Cl_2:CH_3OH) spectra of **1**.

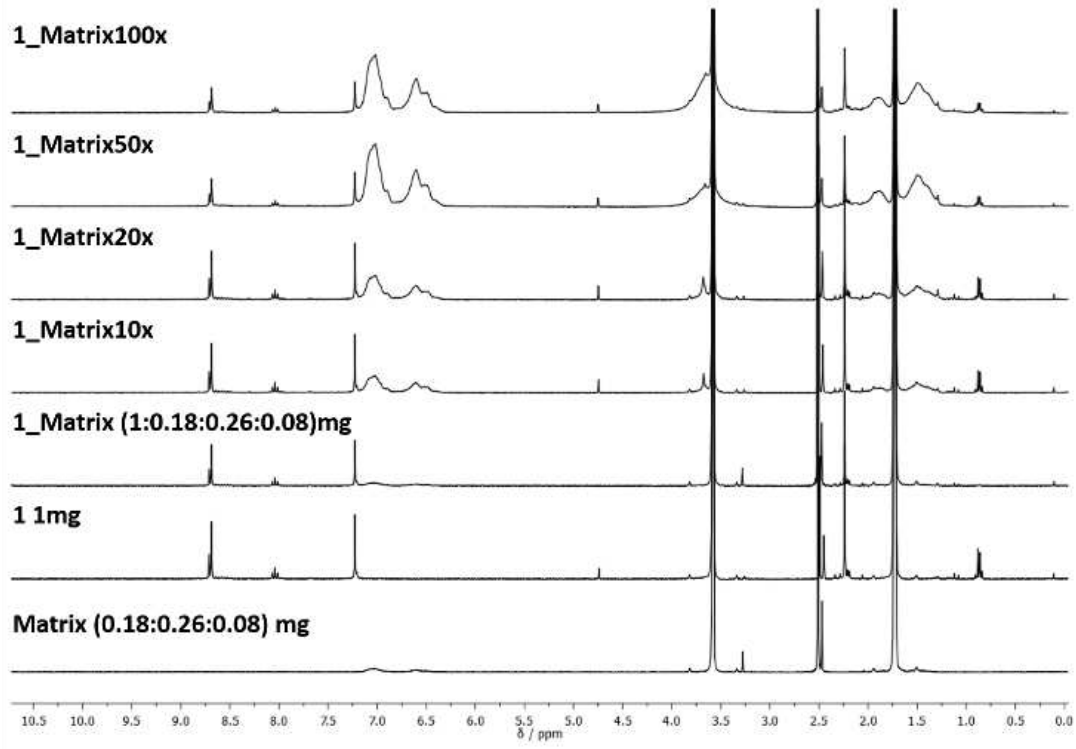
1_Matrix100x
1_Matrix50x
1_Matrix20x
1_Matrix10x
1_Matrix (1:0.18:0.26:0.08)mg
1 1mg
Matrix (0.18:0.26:0.08) mg
10.5 10.0 9.5 9.0 8.5 8.0 7.5 7.0 6.5 6.0 5.5 5.0 4.5 4.0 3.5 3.0 2.5 2.0 1.5 1.0 0.5 0.0
δ / ppm

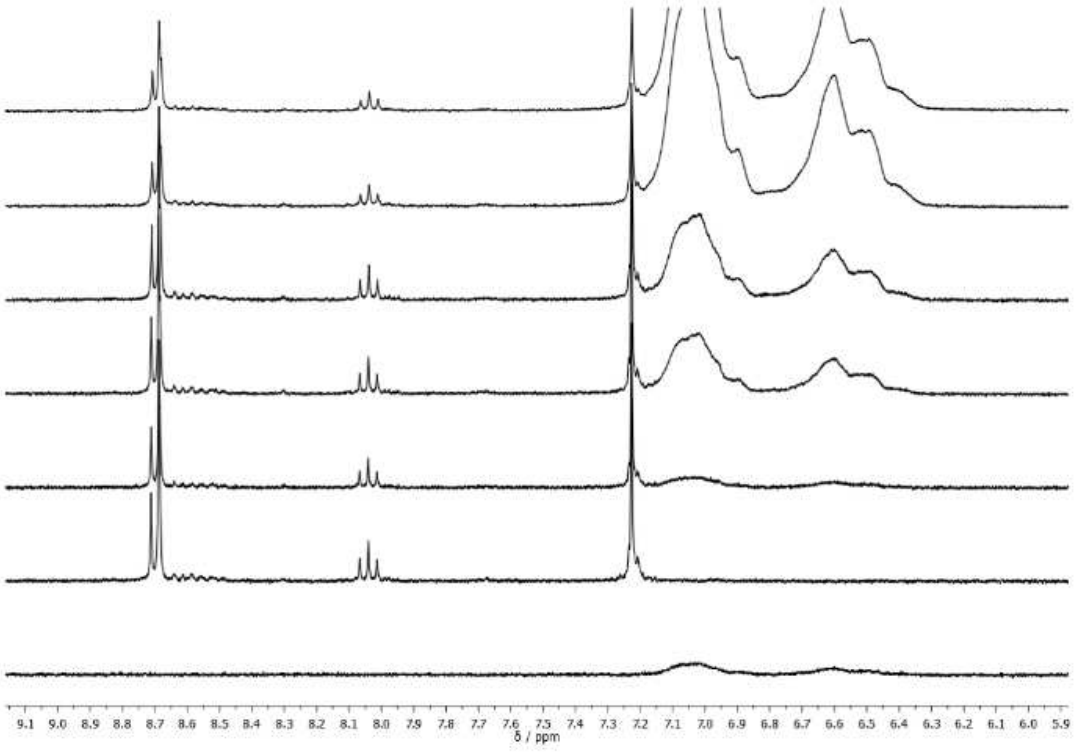
9.1 9.0 8.9 8.8 8.7 8.6 8.5 8.4 8.3 8.2 8.1 8.0 7.9 7.8 7.7 7.6 7.5 7.4 7.3 7.2 7.1 7.0 6.9 6.8 6.7 6.6 6.5 6.4 6.3 6.2 6.1 6.0 5.9
δ / ppm

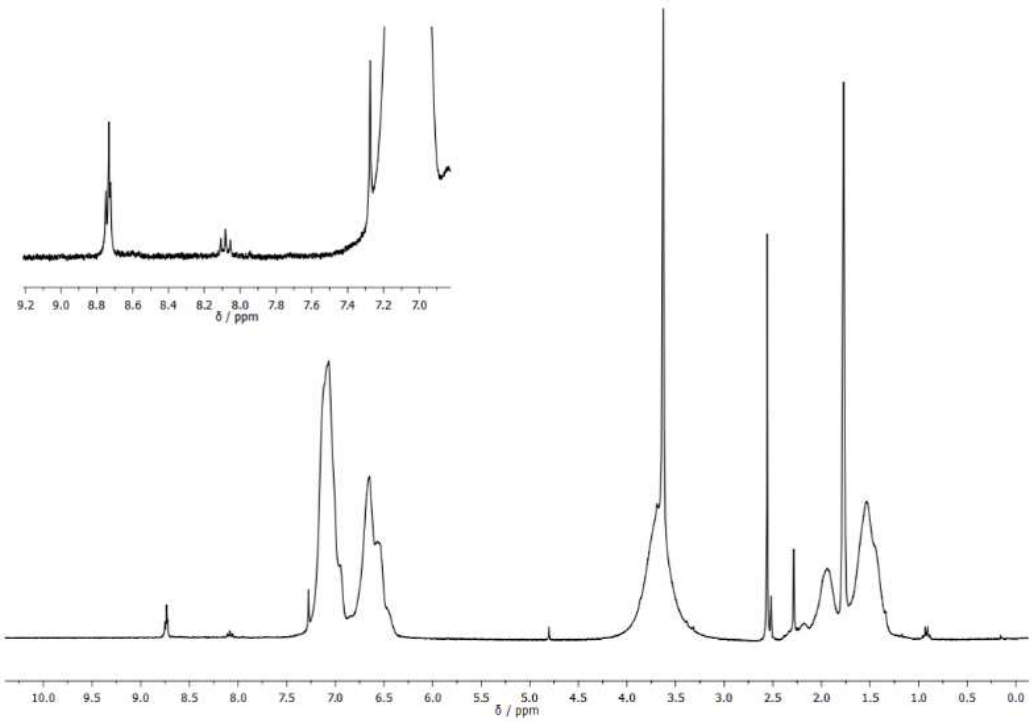

Figure S5. Top: Stacked ^{1}H NMR 300 MHz study in THF-*d*8 showing **1** (1.0 mg) in the presence of increasing amounts of matrix 1×, 10×, 20×, 50× and 100× (starting from 0.18:0.26:0.08 mg PS:PEO:LiOTf). Center: inset on the aromatic region of the spectra highlighting the absence of changes in the signals. Bottom: ^{1}H NMR 300 MHz of the 100× matrix concentration sample after 24h.

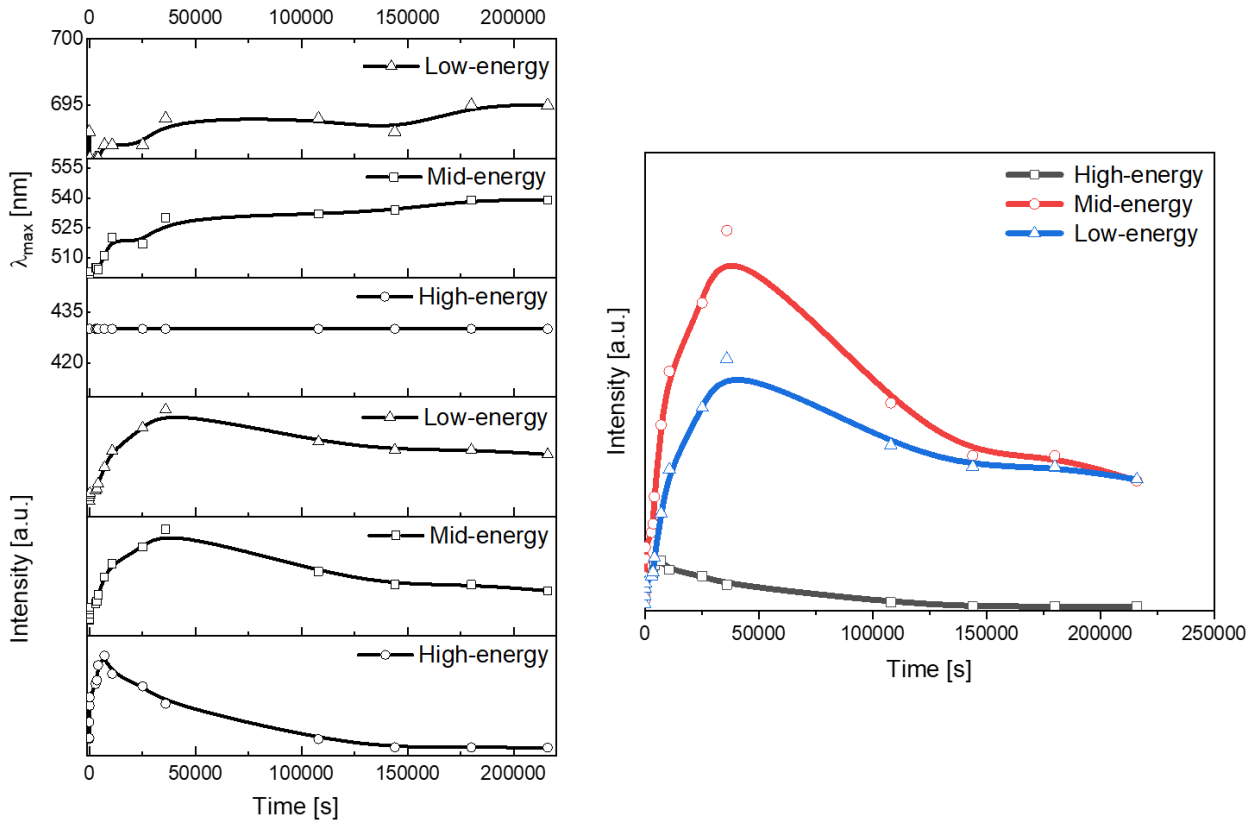

Figure S6. Intensity and λ_{max} changes for the high-, mid-, and low-energy peaks over time of **1**-WLECs driven at pulsed 5 mA.

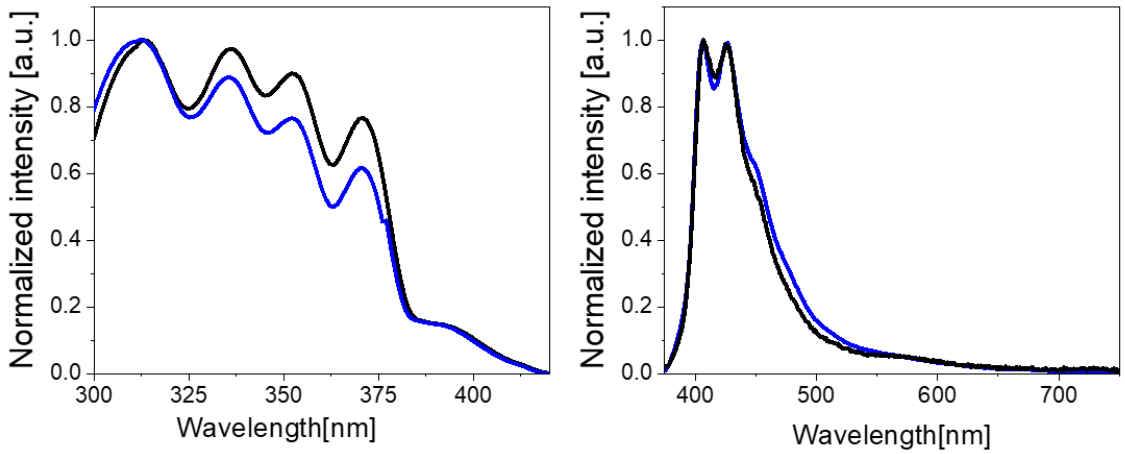

Figure S7. Absorption (left) and emission (right) spectra of fresh (black) and used (blue) devices.

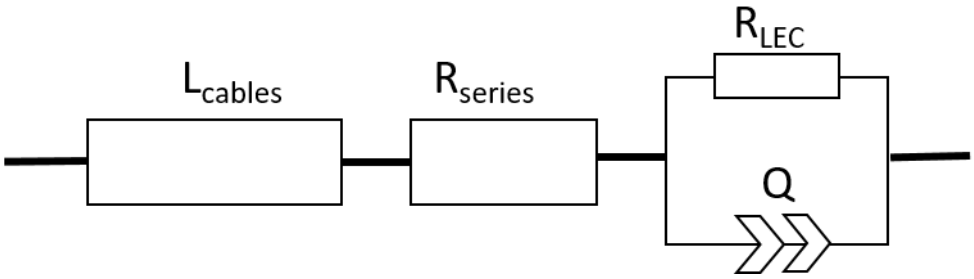

Figure S8. Simplified circuit model with electrical resistance (R_{LEC}) and admittance Q used for static EIS assays. A series resistor (R_{series}) and inductor elements for the cables (L_{cables}) were also included in the model.

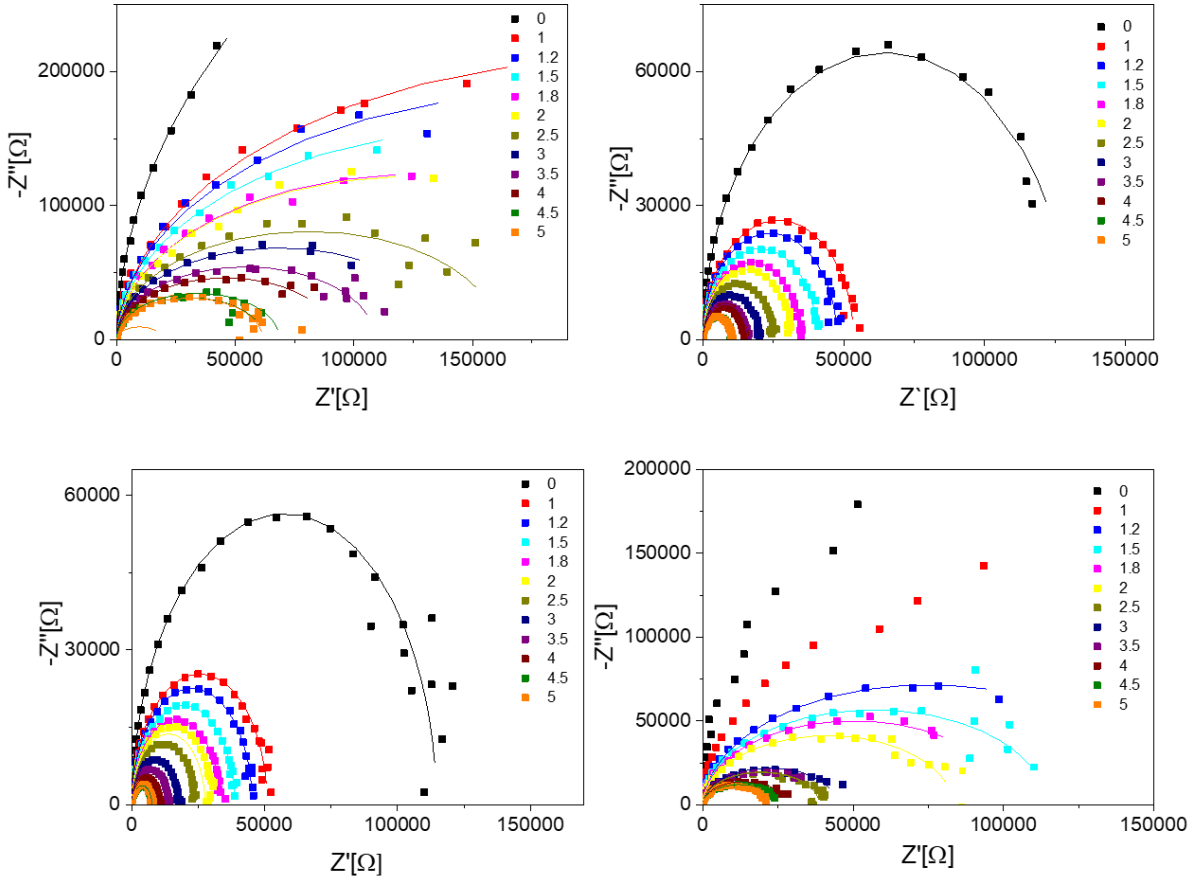

Figure S9. Nyquist plots of fresh (top left), used (top right), used heated at 60°C (bottom left) and used heated at 90°C (bottom right) **1** devices measured upon constant bias (see legend, the values are in V). The fittings are shown in solid lines.

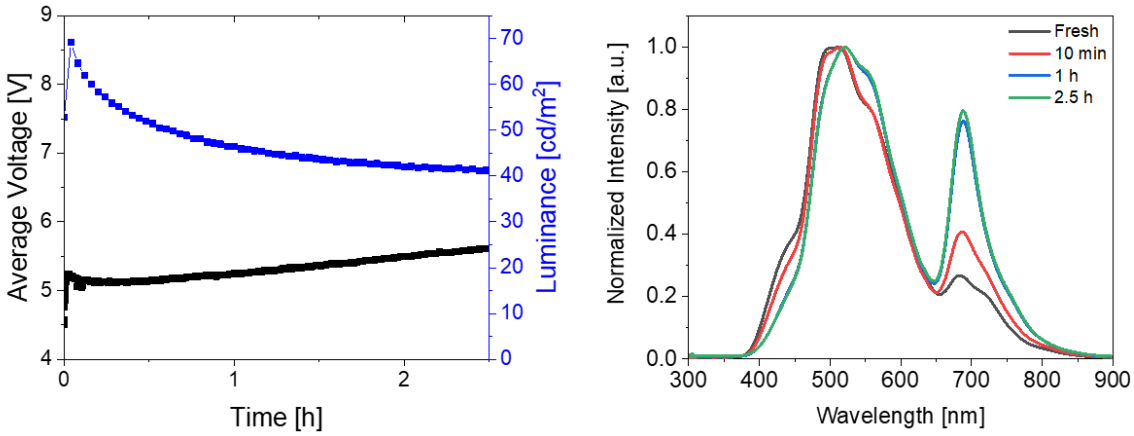

Figure S10. Left: Luminance and applied voltage over time of thin **1**-WLECs driven at pulsed 5 mA. Right: Electroluminescence changes over time highlighted by representative spectra taken at different times (see legends).

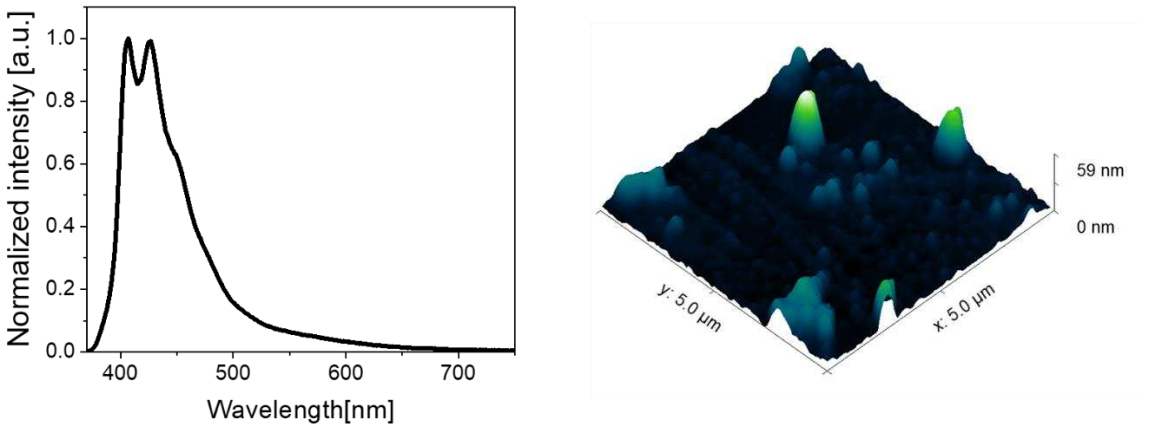

Figure S11. Left: Photoluminescence spectra (λ_{exc}=350 nm) of thin films based on **1**:PEO:LiOTf in air at room temperature. Right: AFM pictures of thin films based on **1**:PEO:LiOTf.

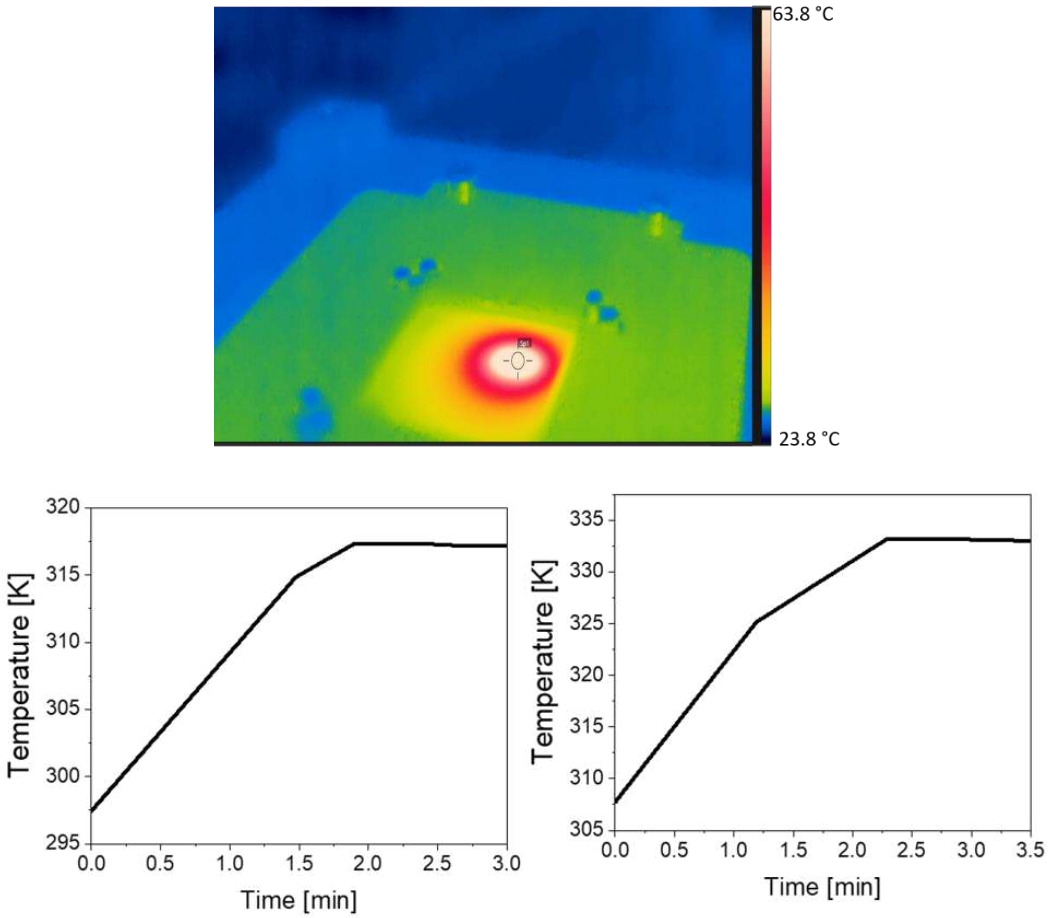

Figure S12. Top: Representative thermal picure of a 1-WLEC operating at pulsed voltage (9V). Bottom: Temperature rise in the first minutes of measurements for thin and thick **1**-WLECs driven at pulsed current of 5 mA (left) and voltage of 9 V (right), respectively.

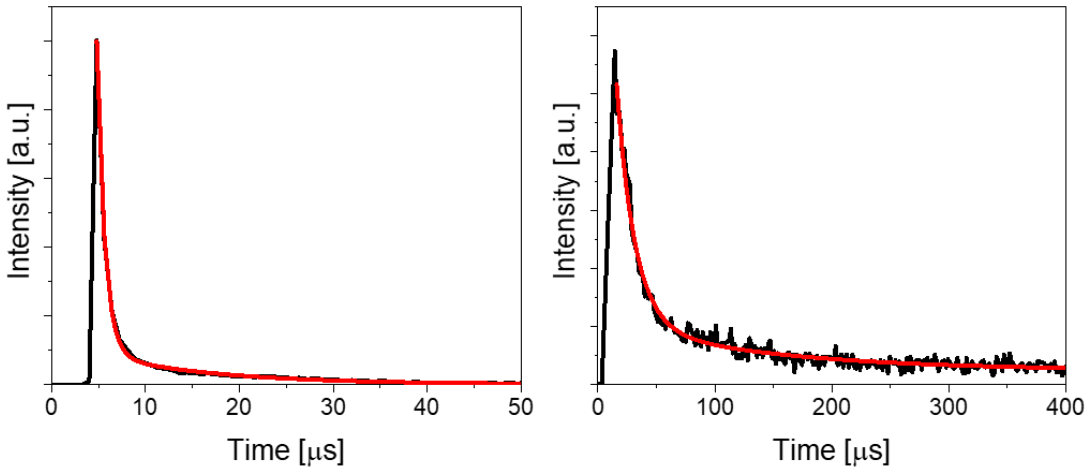

$\langle\tau\rangle$ λ_{max} 550 nm	$\langle\tau\rangle$ λ_{max} 720 nm
5.8 μs	12.3 μs

Figure S13. Excited-state decay profile (λ_{exc} = 355 nm at 60ºC) of **1** films on quartz at λ_{em} of 550 nm (left) and 720 nm (right) and the respective fitting (red). The averaged $\langle\tau\rangle$ are reported below.

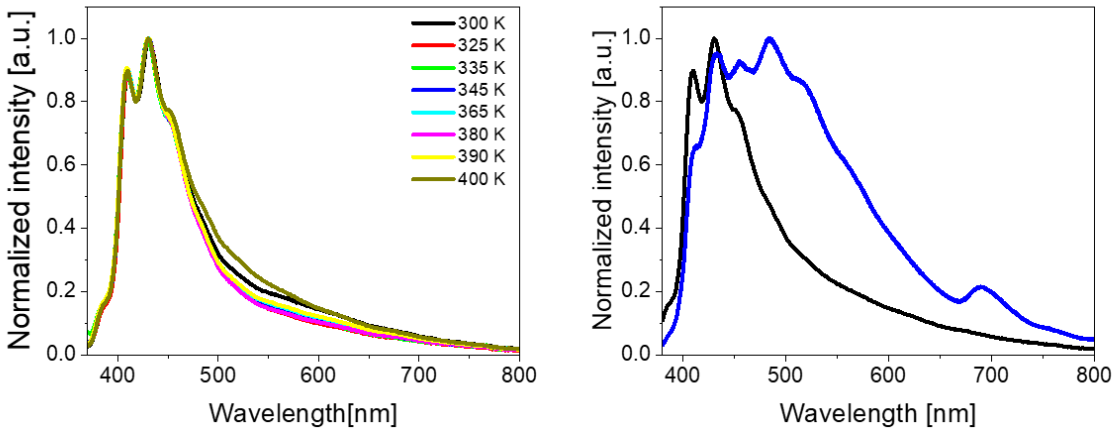

Figure S14. Photoluminescence features of **1** thin films performed in air at different temperatures (left) and comparison at 400 K between the photoluminescence in air (black) and in vacuum (blue).

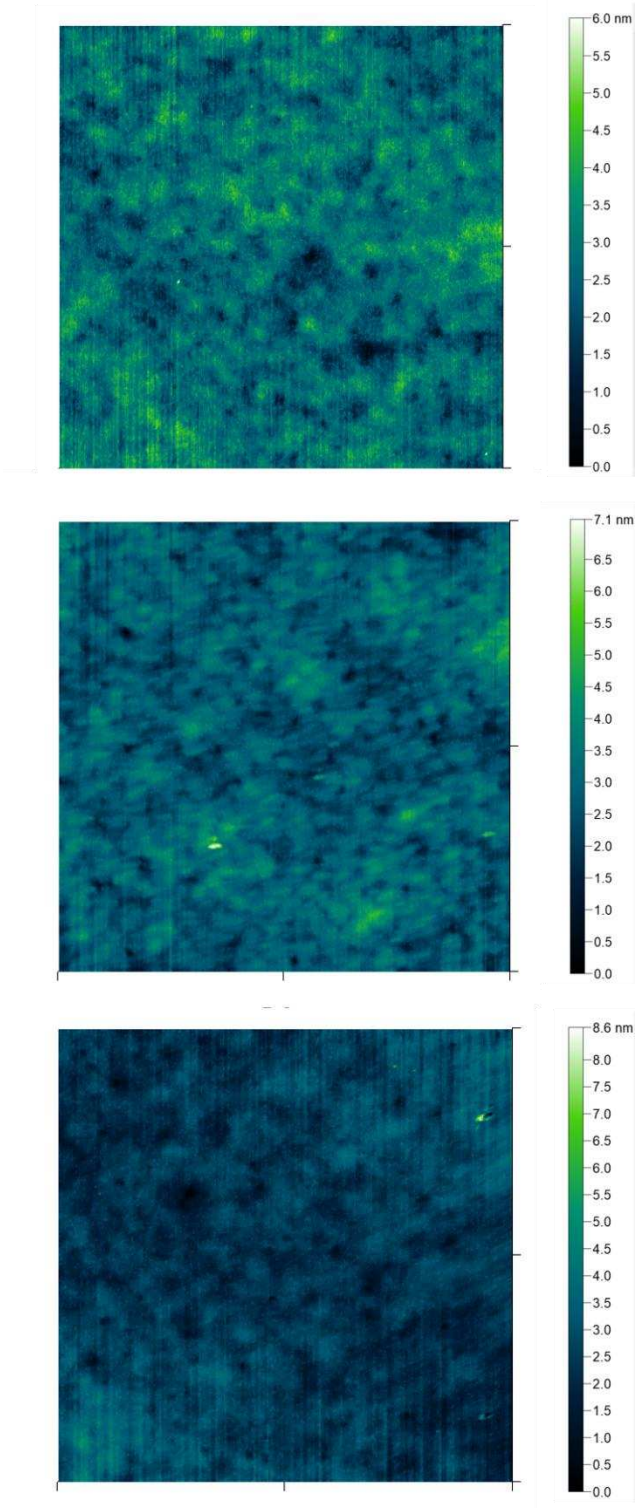

Figure S15. AFM pictures of **1** devices fresh (top), kept at 60°C fresh for 1 day (center), and for 10 days (bottom).

3. Tables

Table S1. Average excited state lifetimes (λ_{exc} = 355 nm at 60 ºC) of **1** devices fresh and kept at 60°C over time.

Time	$<\tau>$ λ_{max} 425 nm	$<\tau>$ λ_{max} 550 nm	$<\tau>$ λ_{max} 720 nm
fresh	3.2 ns	5.9 µs	12.3 µs
1 day	3.1 ns	5.9 µs	12.2 µs
7 days	3.3 ns	5.8 µs	12.2 µs

4. References

[1] J. Dosso, J. Tasseroul, F. Fasano, D. Marinelli, N. Biot, A. Fermi, D. Bonifazi, *Angew. Chem. Int. Ed.* **2017**, *56*, 4483.

[2] C. M. Luk, L. B. Tang, W. F. Zhang, S. F. Yu, K. S. Teng, S. P. Lau, *J. Mater. Chem.* **2012**, *22*, 22378.